ACS APPLIED MATERIALS & INTERFACES

www.acsami.org

Research Article

Understanding the Roles of the Electrode/Electrolyte Interface for Enabling Stable Li||Sulfurized Polyacrylonitrile Batteries

Zhaohui Wu, Seong-Min Bak,* Zulipiya Shadike, Sicen Yu, Enyuan Hu, Xing Xing, Yonghua Du, Xiao-Qing Yang, Haodong Liu,* and Ping Liu*

Cite This: *ACS Appl. Mater. Interfaces* 2021, 13, 31733–31740

Read Online

ACCESS | Metrics & More | Article Recommendations | Supporting Information

ABSTRACT: Sulfurized polyacrylonitrile (SPAN) is a promising high-capacity cathode material. In this work, we use spatially resolved X-ray absorption spectroscopy combined with X-ray fluorescence (XRF) microscopy, X-ray photoelectron spectroscopy, and scanning electron microscopy to examine the structural transformation of SPAN and the critical role of a robust cathode−electrolyte interface (CEI) on the electrode. LiS_x species forms during the cycling of SPAN. However, in carbonate-based electrolytes and ether-based electrolytes with $LiNO_3$ additives, these species are well protected by the CEI and do not dissolve into the electrolytes. In contrast, in an ether-based electrolyte without the $LiNO_3$ additive, LiS_x species dissolve into the electrolyte, resulting in the shuttle effect and capacity loss. Examination of the Li anode by XRF and SEM reveals dense spherical Li morphology in ether-based electrolytes, but sulfur is present in the absence of the $LiNO_3$ additive. In contrast, porous dendritic Li is found in the carbonate electrolyte. These analyses established that an ether-based electrolyte with $LiNO_3$ is a superior choice that enables stable cycling of both electrodes. Based on these insights, we successfully demonstrate the stable cycling of high areal loading SPAN cathode (>6.5 mA h cm^{-2}) with lean electrolyte amounts, showing promising Li||SPAN cell performance under practical conditions.

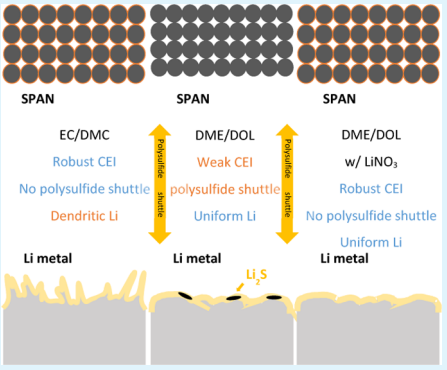

KEYWORDS: *lithium sulfur batteries, sulfurized polyacrylonitrile, Li metal, X-ray fluorescence microscopy, X-ray absorption spectroscopy, lean electrolyte, high energy density*

1. INTRODUCTION

The demands for low-cost and high-energy-density rechargeable batteries for both transportation and large-scale stationary energy storage encourage research to move to "beyond lithium-ion" battery systems such as metal−sulfur, metal−air, and multivalent batteries.[1−6] Since sulfur is a low-cost and abundant material with high theoretical capacity, lithium−sulfur (Li−S) battery chemistry has attracted significant interest during the past decade. The sulfur electrode in Li−S batteries undergoes multiple electron transfer processes associated with long- and short-chain polysulfide (Li_2S_x) intermediates. It is well known that the long-chain polysulfides can dissolve into electrolytes with aprotic organic solvents and migrate to the Li anode side. This so-called "shuttle effect" is considered the main reason for the capacity loss and low coulombic efficiency of the Li−S system.[7,8]

Many efforts have been made to overcome the problem of polysulfide dissolution through advances of sulfur-based materials[9−11] and electrolytes,[12,13] as well as cell engineering.[14] Sulfurized polyacrylonitrile (SPAN) is a promising material due to the confinement of the small molecular sulfur in the conductive polymer network, capable of mitigating polysulfide shuttling.[15] Carbonate electrolytes are widely employed for the Li||SPAN battery, exhibiting excellent chemical compatibility with the SPAN cathode.[16−18] However, the use of carbonate electrolytes results in poor cycling stability of the Li metal anode.[19,20] On the other hand, ether-based electrolytes provide much more stable Li metal anode cycling; the mixed solvent of 1,2-dimethoxyethane (DME) and 1,3-dioxolane (DOL) is employed in most Li metal anode battery research, including Li−S batteries.[21] However, it has been reported that DME/DOL-based electrolytes cause the dissolution of lithium polysulfides from the SPAN and the resulting polysulfide shuttle effect, effectively negating any benefits offered by SPAN.[22,23] Several attempts have been made to improve the stability of SPAN in ether electrolytes either by increasing the salt/solvent ratio or introducing additives.[15,22,24−27] For example, Xing et al.[24] reported that a crystalline cathode−electrolyte interface (CEI) layer composed of LiF and $LiNO_2$ formed by introducing $LiNO_3$ aids in suppressing polysulfide dissolution in a dilute DME-/DOL-based electrolyte. These

Received: April 29, 2021
Accepted: June 24, 2021
Published: July 2, 2021

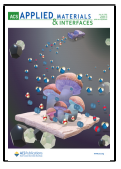

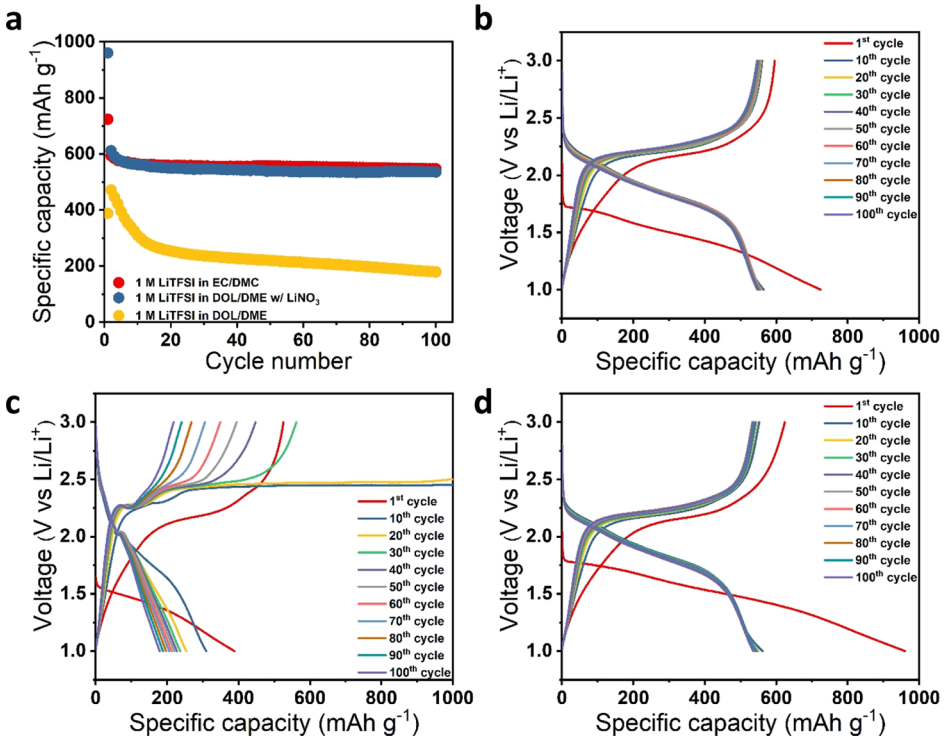

Figure 1. (a) Cycling performance of the SPAN electrode in 1 M LiTFSI-EC/DMC (red dots, CarE), 1 M LiTFSI-DME/DOL (yellow dots, EE), and 1 M LiTFSI-DME/DOL with 0.5 M $LiNO_3$ (blue dots, ENE). Galvanostatic charge and discharge profiles of Li||SPAN coin cell throughout 100 cycles using the electrolyte of 1 M LiTFSI in different electrolyte solvents: (b) CarE, (c) EE, and (d) ENE. The cells were cycled at *C*/5 (1*C* = 550 mA h g^{-1}).

works mainly focused on improving the performance of Li||SPAN cells, with little understanding of the conversion of sulfur in SPAN during the electrochemical cycling process and the roles of the electrode−electrolyte interfaces on retaining the sulfur species in the SPAN cathode.

In this report, we investigate the performance and working mechanisms of Li||SPAN batteries in three different electrolytes: 1 M LiTFSI in EC/DMC (CarE), 1 M LiTFSI in DME/DOL (EE), and 1 M LiTFSI and 0.5 M $LiNO_3$ in DME/DOL (ENE) that enable stable cycling of SPAN, Li, and both SPAN and Li, respectively. To probe the fate of the sulfur-containing species in different electrolytes, a spatially resolved X-ray absorption spectroscopy (XAS) combined with X-ray fluorescence (XRF) microscopy characterization technique is utilized. The morphological changes and the redistribution of sulfur and polysulfide in both the SPAN cathode and lithium metal anode are monitored through the XRF images, while the chemical-state changes of the S in SPAN and sulfur-containing interfacial layer are characterized with XAS. Coupled with X-ray photoelectron spectroscopy (XPS) and scanning electron microscopy (SEM), the results in this study provide an in-depth understanding of the reaction processes and the key roles of the CEI and SEI for stabilizing the SPAN and Li electrodes. Besides the enhanced fundamental understandings, the stable cycling of a high areal loading SPAN cathode (>6.5 mA h cm^{-2}) with a lean electrolyte amount of 3 g A h^{-1} is successfully demonstrated in the ENE electrolyte with a LiF-rich CEI. In contrast, the Li||SPAN cell using CarE shorted during its fourth cycle. The excellent performance of our Li||SPAN cell paves the way for the development of practical high-energy-density Li||SPAN batteries.

2. RESULTS AND DISCUSSION

We first compare the electrochemical performance of SPAN in three different electrolytes (Figure 1). The areal capacity of the SPAN electrode is ∼1 mA h cm^{-2}. The volume of the electrolyte is 75 μL in order to investigate the compatibility between electrolytes and the SPAN material. SPAN shows stable cycling in CarE at *C*/5 between 1 and 3 V, consistent with previous reports.[16] The electrode maintains a reversible capacity of ∼550 mA h g^{-1} after 100 cycles (Figure 1b). However, the SPAN material does not cycle well in the EE electrolyte. There is a long charge plateau at ∼ 2.4 V, indicating that the shuttling reaction of Li_2S_n takes place in this ether electrolyte, resulting in active sulfur loss from the SPAN and low coulombic efficiency (Figures 1c and S1). Within 10 cycles, its capacity decreases from 471 to 309 mA h g^{-1}. With the addition of 0.5 M $LiNO_3$ to form the ENE electrolyte, the charge plateau related to the polysulfide shuttle is effectively eliminated (Figure 1d). The ENE electrolyte shows high coulombic efficiency toward both the Li anode (>98%) and SPAN cathode (∼100%), as shown in Figure S2. Besides the high coulombic efficiency, the cell delivers a capacity of 536 mA h g^{-1} at its 100th cycle, corresponding to a capacity retention rate of 93.2% (based on the capacity at the fifth cycle).

Evidently, the SPAN performs differently in carbonate- and ether-based electrolytes. We hypothesized that the presence of a CEI layer on the SPAN cathode is the key to enabling the stable cycling of SPAN in ENE. XPS was conducted on SPAN electrodes after five cycles and in a charged (delithiated) state to examine the compositions of the CEI formed in different electrolytes. The C 1s spectra (Figure 2a−c) show that the O−C═O and C−O peaks dominate the C 1s region of SPAN

https://doi.org/10.1021/acsami.1c07903
ACS Appl. Mater. Interfaces 2021, 13, 31733−31740

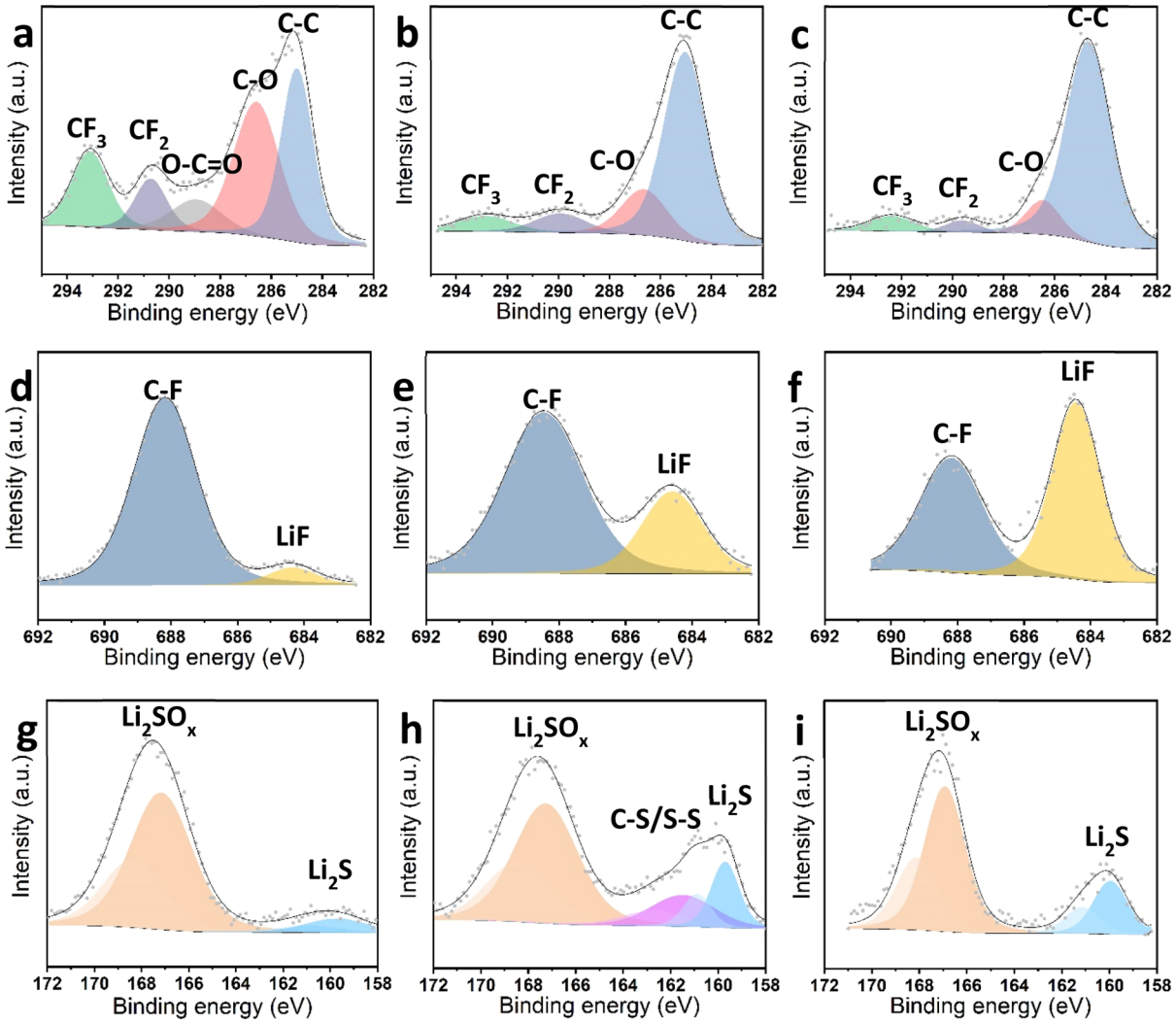

Figure 2. XPS of the cycled SPAN cathode. C 1s spectra in (a) CarE, (b) EE, and (c) ENE. F 1s spectra (d) CarE, (e) EE, and (f) ENE. S 2p spectra in (g) CarE, (h) EE, and (i) ENE.

cycled in CarE, likely due to the decomposition of carbonate solvents to form a RCO_3Li-rich CEI, where R is an alkyl group.[28,29] In contrast, the decomposition of the ether on the SPAN cathode is negligible. Both C−F and LiF peaks are observed in all three cases (Figure 2d−f). The C−F bond is attributed to the PVdF binder, while the LiF derived from the LiTFSI salt is the CEI component.[30] The SPAN electrode from the ENE showed a significantly higher LiF concentration in its CEI layer. A LiF-rich CEI on the SPAN electrode surface is believed to prevent polysulfide dissolution.[24] Figure 2g−i shows the S 2p spectra of the cycled SPAN electrodes. Doublets at around 168 and 160 eV are assigned to Li_2SO_x and Li_2S, which are observed in all three electrolyte systems.[24] However, the C−S/S−S signals from SPAN are found only on the SPAN electrode cycled in EE.[31] This indicates that polysulfide dissolution takes place in EE due to the lack of a LiF-rich CEI as the protective layer, while the RCO_3Li-rich CEI in the carbonate electrolyte prevents the detection of the underlying SPAN structure.

To further investigate how the sulfur-based species evolve in the SPAN electrodes, we utilized a combined XRF and S K-edge XAS technique, which not only provides global elemental distribution over the electrode at the millimeter length scale but also probes the spatially resolved chemical information of sulfur-based species using the microsized beam. Figure 3a shows an XRF image of a pristine SPAN cathode (2×4 mm^2 area) measured at an incident X-ray beam energy of 2480 eV. An inhomogeneous distribution of sulfur-based species is observed, as depicted with circles for high- and low-S concentration areas in Figure 3a. The corresponding XAS spectra of the selected areas are shown in Figure 3b. The absorption intensity, so-called the "edge-jump", indicates the total absorption of sulfur species at the spot where the microsized beam [16 μm (horizontal) × 5 μm (vertical)] shined. For a more detailed investigation of the chemical state, the XAS plot is normalized, as shown in Figure 3c. A spectral distortion is observed at the XANES, which should be mainly caused by self-absorption due to the high sulfur concentration for the spectrum collected from the high S area. Except for the spectral distortion, the chemical status of the pristine SPAN cathode is uniform and only has a slight thickness variation that might have been induced by the slurry casting process used for electrode fabrication. Both spectra represent the same three major peaks as indicated: 1 (2468.5 eV), 2 (2470.8 eV), and 3 (2472.5 eV) (Figure 3c). These peaks can be attributed to the transition from S 1s to S=C π^*, S−S σ^*, and S−C σ^*

https://doi.org/10.1021/acsami.1c07903
ACS Appl. Mater. Interfaces 2021, 13, 31733−31740

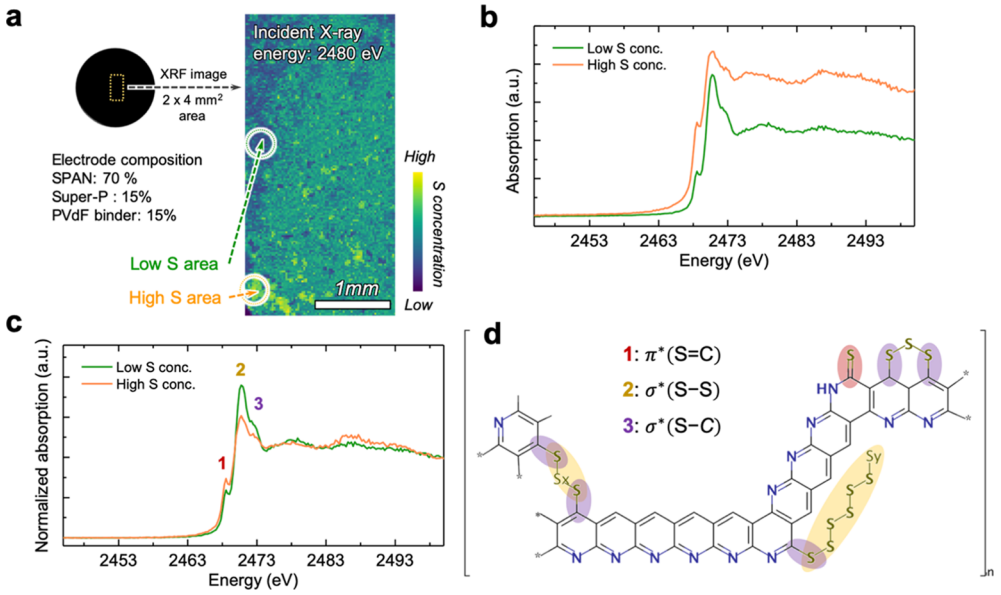

Figure 3. (a) XRF image of pristine SPAN cathode measured at incident X-ray beam energy of 2480 eV with indications of inhomogeneous distribution of sulfur-containing chemical species, (b) measured S K-edge μXANES spectra at the selected area for low and high S concentration indicated in the XRF image. (c) Normalized S K-edge μXANES spectra and (d) model structure of SPAN redrawn based on the previous report by Fanous et al.[34] All of the red, yellow, and purple regions indicating that S═C, S−S, and S−C bonds exist in the SPAN in this study.

states in the SPAN structure, respectively.[32,33] The corresponding bonding structure is displayed with a colored circle over the SPAN structure in Figure 3d. The proposed structure in Figure 3d is adopted from the previous report by Fanous et al.[34] We note that this model is only one of several structures that have been proposed,[23,35−37] which might be due to the variance of the synthesis route and the resulting complexity of the polymeric structure of SPAN. Although the proposed structures differ in detail, all of them incorporate covalent bonding between sulfur and carbon in the SPAN, instead of the physical absorption of elemental sulfur in carbon. In this study, we use the structure in Figure 3d for the following discussions, which is consistent with the observed result from the XAS data.

Figure 4a shows the XRF images for SPAN cathodes after five cycles and in a charged (delithiated) state with different electrolytes. XRF images were collected at two different incident X-ray energies of 2469 and 2480 eV. The images collected at 2469 eV represent the chemical states of low valence S (e.g., S═C π*, Li_2S_x) only, while the images collected at 2480 eV are used for representing excitations of all sulfur states available below 2480 eV. Interestingly, a lower-S-concentration area (dark blue color region) is observed for the EE case at the 2469 eV, whereas no noticeable difference is observed at 2480 eV. This indicates that the transition-allowed states for the pre-edge region in the EE case are diminished, which implies a reduced concentration of S═C π* (or low valence state S such as LiS_x). The corresponding XAS spectra for each selected area are shown in Figure 4b, which contain three distinct peaks featured at around 2469, 2471, and 2478 eV. All the electrodes show a uniform S distribution with almost no variance in each spectrum, while some variations in peak developments are observed in different electrolyte systems.

A more detailed analysis of the chemical states can be performed with normalized XAS spectra in Figure 4c. By comparing the spectra with that of pristine SPAN, several

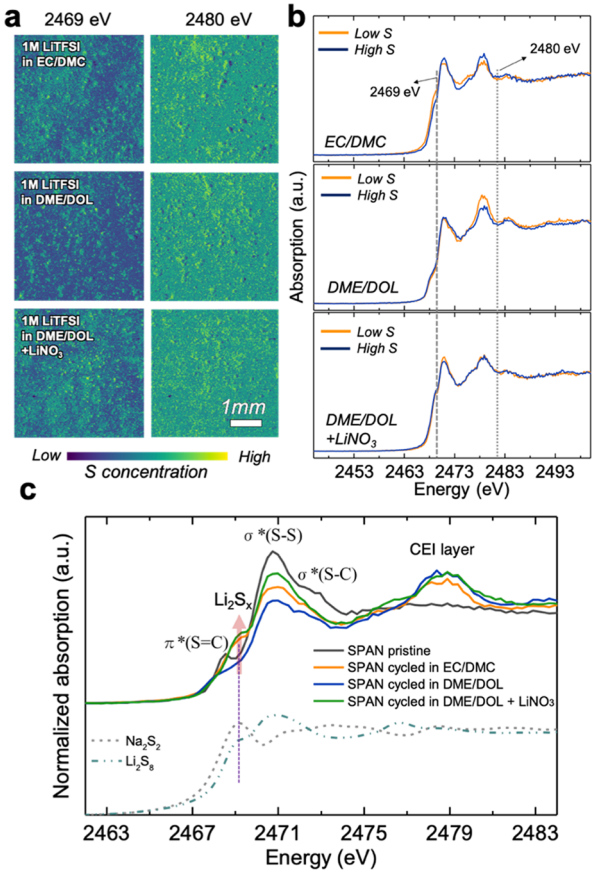

Figure 4. (a) XRF image of SPAN cathodes (4 × 4 mm^2 area) cycled in EC/DMC, DME/DOL, DME/DOL with $LiNO_3$, measured with an incident beam energy of 2469 and 2480 eV. (b) Corresponding S K-edge XANES spectra were measured at low and high S concentration regions chosen from (a). (c) Normalized S K-edge XANES spectra for comparison with reference spectra of Na_2S_2 and Li_2S_8.[41]

https://doi.org/10.1021/acsami.1c07903
ACS Appl. Mater. Interfaces 2021, 13, 31733−31740

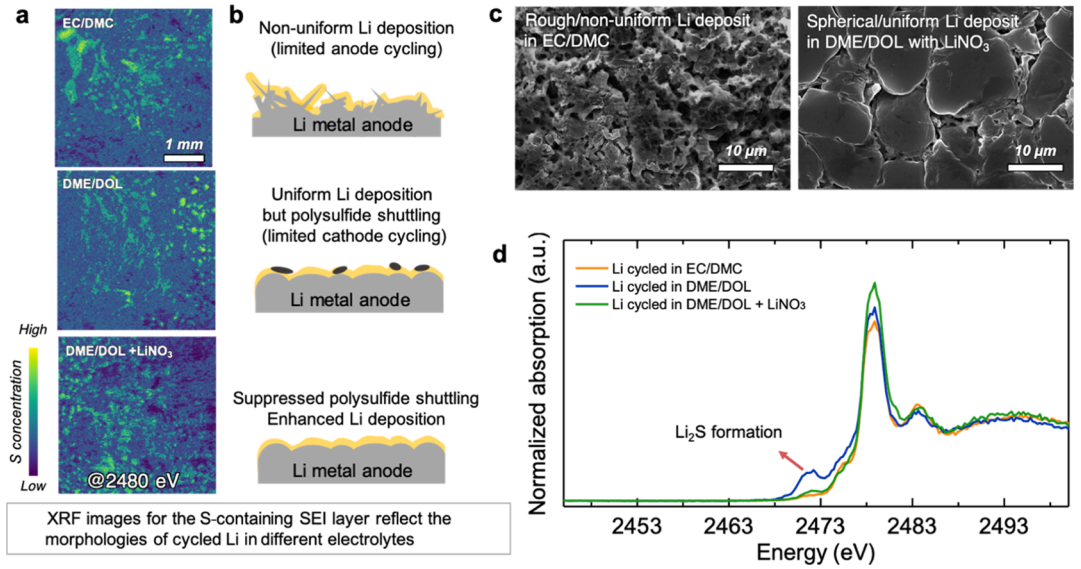

Figure 5. (a) XRF image of Li metal anodes cycled in CarE, EE, and ENE, measured at an incident beam energy of 2480 eV. (b) Corresponding schematic sketch of a cross-sectional view of the Li metal anode for each case and (c) SEM images for the Li metal anode after 100 cycles in CarE and ENE. (d) Normalized S K-XANES measured from the selected area from (a).

distinct peak changes could be observed. First, the S═C π^* peak of SPAN diminishes in all electrolytes after cycling, which does not fully recover to its initial status, reflecting the irreversible cleavage of the S═C bond. Further investigation on the irreversible cleavage of the S═C was made with the SPAN electrode at a fully discharged state (at 1.0 V vs Li/Li^+) and fully charged state after the first cycle (at 3.0 V vs Li/Li^+) in EE or ENE. As shown in Figure S3a,b, the peak for the S═C bond disappears, regardless of CEI composition at the fully discharged state. The S═C bond is only partially recovered during the charging process, which might lead to the irreversible capacity loss during the first cycle. Additionally, in contrast to the EE case, a new peak associated with Li_2S_x appeared after first charge for the cases of CarE and ENE. Notably, the Li_2S_x peak is enhanced upon cycling in the presence of $LiNO_3$ (Figure S3b), indicating the accumulation of Li_2S_x on the SPAN cathode during the cycling. The lack of Li_2S_x for the EE electrolyte implies dissolution of Li_2S_x into the electrolyte rather than being retained in the SPAN cathode.[38] This is a direct evidence of the polysulfides Li_2S_x dissolution that might result in polysulfide shuttling. The shuttling of polysulfide is also confirmed by cross-checking the Li metal surface, which will be discussed later.

We next analyze the spectra in Figure 4c in the energy range of around 2471 eV, where the absorption peak intensities of the S−S bond and S−C bond decrease after five cycles. A change of these peaks is associated with radical-type SPAN formation with cleavage of the S−S and S−C bonds in the SPAN structure during the first cycle.[36] A dissolution or loss of sulfur units from the SPAN molecules may also be involved, and it appears as a more considerable decrease of the S−S bond in the XANES spectrum for the electrode cycled in EE. Finally, a broad peak with a center at around 2478 eV, which we attribute to the CEI, appears for all the samples. The broad peak for the CEI over the wide range of energy is attributed to the transition from the 1s to the S−O σ^* state in the oxidized sulfur species such as $-SO_3^{2-}$ (2477 eV), $-COSO^{2-}$ (2479 eV), and $-SO_4^{2-}$ (2482 eV).[39−42]

Investigation of cycled SPAN cathodes from different electrolytes has addressed the following points regarding the structural changes of SPAN and the role of a LiF-rich CEI in the ether electrolyte: (1) the first cycle irreversible reaction is associated with the irreversible cleavage of S═C and S−C bonds in the SPAN structure; (2) lithium polysulfide, Li_2S_x, forms in the cathode after the first full cycle. In the EE electrolyte, the decrease of the S−S bond and the Li_2S_x peak reveals that the fast capacity degradation of SPAN in EE is caused by the Li_2S_x dissolution and shuttling; (3) in contrast, the Li_2S_x peak is stable in CarE and ENE due to the formation of a LiF-rich CEI, which explains the stable cycling of SPAN in these two electrolytes. The LiF-rich CEI serves as a protective layer for the SPAN cathode to prevent the Li_2S_x from dissolving into the EE.[36]

In order to probe the effect of electrolytes on the anode, we also collected XRF images and XAS on the Li electrode surface. Although the XAS is not a technique capable of directly probing the Li metal due to the low energy characteristic of Li, the sulfur-containing solid electrolyte interface (SEI) layer can be characterized with S K-edge XAS. Moreover, XRF imaging at 2480 eV can visualize the SEI layer that reflects the morphology of lithium metal underneath it. The XRF images for the cycled lithium metal anode in the different electrolytes are shown in Figure 5a. Nonuniform and rough shapes of Li deposition are observed for the lithium anode cycled in CarE, while spherical and relatively uniform Li deposition is observed in EE and ENE. A schematic sketch of a cross-sectional view of the lithium metal for each case is shown in Figure 5b. Figure 5c shows the morphology of lithium after 100 cycles in CarE and ENE electrolytes. The lithium in CarE developed a mossy appearance, while the lithium in ENE electrolyte deposited as large grains with a relatively regular round shape. The better morphology is typically associated with higher coulombic efficiency of the Li anode[43−46] because a more compact lithium deposition would result in a more uniform and efficient stripping in the next charging cycle.

The corresponding XAS spectra are plotted in Figure 5d. The highest-intensity peak at 2479 eV corresponds to the SEI

https://doi.org/10.1021/acsami.1c07903
ACS Appl. Mater. Interfaces 2021, 13, 31733−31740

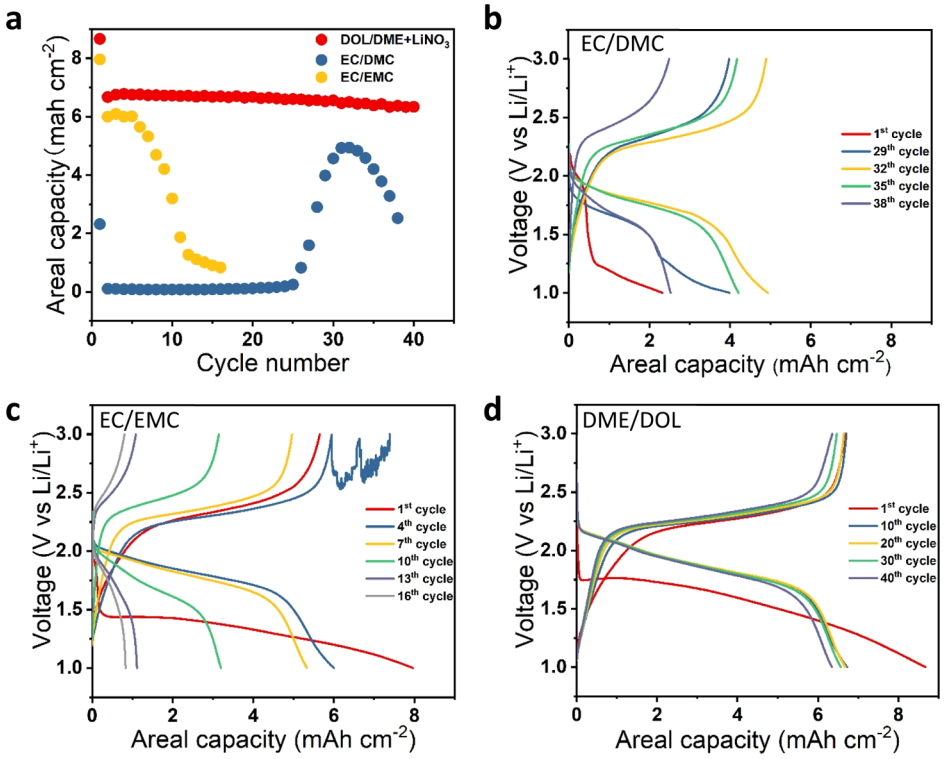

Figure 6. (a) Lean electrolyte (3 g A h^{-1}) cycling performance of a thick SPAN electrode in carbonates and DME/DOL with $LiNO_3$. (b) Voltage profile in 1 M LiTFSI-EC/DMC. (c) Voltage profile in 1 M LiTFSI-EC/EMC. (d) Voltage profile in 1 M LiTFSI-DME/DOL with 0.5 M $LiNO_3$. The cells were cycled at *C*/5 (1*C* = 550 mA h g^{-1}).

layer, including oxidized sulfur species such as $-COSO_2$, a product of electrolyte decomposition.[40] A small peak of Li_2S appears just below 2473 eV in the case of EE. Li_2S, which is the final product of the conversion of lithiated sulfur, can be formed only through the shuttling of Li_2S_x from the cathode side. In contrast, the electrode cycled in ENE shows no Li_2S peak. This result confirms that the LiF-rich CEI could effectively suppress the polysulfide shuttle in the EE electrolyte.

The SPAN electrode with an areal capacity of 1 mA h cm^{-2} shows stable cycling in both CarE and ENE. To further elucidate the benefits of the ENE electrolyte under a more realistic battery testing condition, we tested a high-areal-capacity SPAN electrode under lean electrolyte conditions, an important step toward realizing cells with high energy density. As shown in Figure 6a, when the electrolyte amount was reduced to 3 g A h^{-1}, the cell with CarE initially was unable to deliver any capacity due to the poor wettability of EC/DMC. It took 25 cycles to activate the thick SPAN electrode, but its capacity quickly decayed due to the consumption of the electrolyte. We also conducted the same experiment with 1 M LiTFSI-EC/EMC, which shows a significant improvement in wettability. The cell initially delivered a reversible capacity of 6 mA h cm^{-2}. However, it suffered from soft shorting in the fourth cycle, as indicated by the fluctuating voltage profile in Figure 6c.

While the high-loading SPAN cells with lean carbonate electrolyte either shorted quickly or experienced fast capacity decay, the lean ENE electrolyte cell with the help of the LiF-rich CEI showed very stable cycling for 40 cycles, as displayed in Figure 6d. The electrode delivers an initial reversible capacity of 6.67 mA h cm^{-2}, which still maintains 6.34 mA h cm^{-2} in the 40th cycle. In terms of the voltage profiles, the CarE electrolyte cell shows rapid polarization increase, while the ENE one is relatively stable. The amplified difference in cycling stability arises from the difference in lithium morphology. When the mossy morphology is formed in the carbonate electrolyte, the porous lithium requires an electrolyte to fill the pores, a major issue with lean electrolyte conditions. The cell impedance will quickly rise as a consequence of electrolyte consumption. In addition, the dendritic morphology in the carbonate electrolyte could also result in internal shorts, as shown in the 1 M LiTFSI-EC/EMC electrolyte. The deposition of large lithium grains in the ENE electrolyte combined with the LiF-rich CEI enabled stable cycling of the high-areal-capacity SPAN electrode cycled under lean electrolyte conditions.

3. CONCLUSIONS

In conclusion, we have conducted detailed structural, chemical, and electrochemical analysis of Li||SPAN cells with three electrolytes, CarE that enables stable cycling of SPAN but not Li, EE that enables stable cycling of Li but not SPAN, and ENE that allows both electrodes to cycle stably. XPS results have revealed the formation of a robust LiF-rich CEI layer in the ENE. The role of the LiF-rich CEI layer has been further explored with the S K-edge spatially resolved XAS/XRF, which reveals the formation of Li_2S_x on the SPAN cathode after one discharge−charge cycle. In the EE electrolyte, Li_2S_x diffuses to the Li anode and covers the Li surface in its reduced form of Li_2S. In ENE, a robust LiF-rich CEI on the SPAN cathode enables effective prevention of Li_2S_x shuttling and retaining Li_2S_x on the SPAN cathode, as evidenced by the absence of Li_2S formation on the Li metal anode. Leveraging the good compatibility between Li and ether-based electrolyte and our

https://doi.org/10.1021/acsami.1c07903
ACS Appl. Mater. Interfaces 2021, 13, 31733−31740

improved understanding in the role of the LiF-rich CEI, we are able to realize a stable-cycling and high-energy-density Li||SPAN cell with a high areal loading SPAN cathode (>6.5 mA h cm^{-2}) and a lean electrolyte amount of 3 g A h^{-1} that shows 40 stable cycles in the ENE electrolyte. Our work proves the benefits of using an ether electrolyte with nitrate additives for Li||SPAN cells under a high-loading, lean-electrolyte condition and advances the understanding of the critical roles of electrode/electrolyte interfaces on enabling stable cycling of SPAN.

■ ASSOCIATED CONTENT

Supporting Information

The Supporting Information is available free of charge at https://pubs.acs.org/doi/10.1021/acsami.1c07903.

Experimental methods and normalized S K-edge XANES for pristine and cycled SPAN cathodes (PDF)

■ AUTHOR INFORMATION

Corresponding Authors

Seong-Min Bak − *National Synchrotron Light Source II, Brookhaven National Laboratory, Upton, New York 11973, United States;* orcid.org/0000-0002-1626-5949; Email: smbak@bnl.gov

Haodong Liu − *Department of NanoEngineering, University of California San Diego, La Jolla, California 92093, United States; Center for Memory and Recording Research, University of California San Diego, La Jolla, California 92093, United States*; Email: hal055@eng.ucsd.edu

Ping Liu − *Department of NanoEngineering, University of California San Diego, La Jolla, California 92093, United States;* orcid.org/0000-0002-1488-1668; Email: piliu@eng.ucsd.edu

Authors

Zhaohui Wu − *Department of NanoEngineering, University of California San Diego, La Jolla, California 92093, United States;* orcid.org/0000-0002-1453-6784

Zulipiya Shadike − *Chemistry Division, Brookhaven National Laboratory, Upton, New York 11973, United States;* orcid.org/0000-0001-9140-7495

Sicen Yu − *Program of Material Science, University of California San Diego, La Jolla, California 92093, United States*

Enyuan Hu − *Chemistry Division, Brookhaven National Laboratory, Upton, New York 11973, United States;* orcid.org/0000-0002-1881-4534

Xing Xing − *Program of Material Science, University of California San Diego, La Jolla, California 92093, United States*

Yonghua Du − *National Synchrotron Light Source II, Brookhaven National Laboratory, Upton, New York 11973, United States*

Xiao-Qing Yang − *Chemistry Division, Brookhaven National Laboratory, Upton, New York 11973, United States;* orcid.org/0000-0002-3625-3478

Complete contact information is available at: https://pubs.acs.org/10.1021/acsami.1c07903

Author Contributions

P.L. and H.L. conceived the idea. Z.W. synthesized the material. Z.W. and X.X. performed electrochemical experiments. S.Y. conducted the XPS experiment. S.-M. B., Z.S., E.H., Y.D., and X.Y. conducted the XAS and XRF experiments and analysis. All authors contributed to the writing of the manuscript and have given approval to the final version of the manuscript.

Notes

The authors declare no competing financial interest.

■ ACKNOWLEDGMENTS

The work done at Brookhaven National Laboratory was supported by the Assistant Secretary for Energy Efficiency and Renewable Energy, Vehicle Technology Office of the U.S. DOE, through the Advanced Battery Materials Research (BMR) Program, including Battery500 Consortium under contract DE-SC0012704. This research used beamline 8-BM (TES) of the National Synchrotron Light Source II, U.S. DOE Office of Science User Facilities, operated for the DOE Office of Science by Brookhaven National Laboratory under contract no. DE-SC0012704. The work done at UC San Diego was supported by the Office of Vehicle Technologies of the U.S. Department of Energy through the Advanced Battery Materials Research (BMR) Program (Battery500 Consortium) under contract no. DE-EE0007764. Part of the work used the UCSD-MTI Battery Fabrication Facility and the UCSD-Arbin Battery Testing Facility.

■ REFERENCES

(1) Wu, F.; Yushin, G. Conversion Cathodes for Rechargeable Lithium and Lithium-Ion Batteries. *Energy Environ. Sci.* **2017**, *10*, 435−459.

(2) Fang, R.; Xu, J.; Wang, D.-W. Covalent Fixing of Sulfur in Metal-Sulfur Batteries. *Energy Environ. Sci.* **2020**, *13*, 432−471.

(3) Zhang, X.; Chen, K.; Sun, Z.; Hu, G.; Xiao, R.; Cheng, H.-M.; Li, F. Structure-Related Electrochemical Performance of Organosulfur Compounds for Lithium-Sulfur Batteries. *Energy Environ. Sci.* **2020**, *13*, 1076.

(4) Rahman, M. A.; Wang, X.; Wen, C. High Energy Density Metal-Air Batteries: A Review. *J. Electrochem. Soc.* **2013**, *160*, A1759−A1771.

(5) Ponrouch, A.; Bitenc, J.; Dominko, R.; Lindahl, N.; Johansson, P.; Palacin, M. R. Multivalent Rechargeable Batteries. *Energy Storage Mater.* **2019**, *20*, 253−262.

(6) Liu, J.; Bao, Z.; Cui, Y.; Dufek, E. J.; Goodenough, J. B.; Khalifah, P.; Li, Q.; Liaw, B. Y.; Liu, P.; Manthiram, A.; Meng, Y. S.; Subramanian, V. R.; Toney, M. F.; Viswanathan, V. V.; Whittingham, M. S.; Xiao, J.; Xu, W.; Yang, J.; Yang, X.; Zhang, J. Pathways for Practical High-Energy Long-Cycling Lithium Metal Batteries. *Nat. Energy* **2019**, *4*, 180−186.

(7) Liu, T.; Hu, H.; Ding, X.; Yuan, H.; Jin, C.; Nai, J.; Liu, Y.; Wang, Y.; Wan, Y.; Tao, X. 12 Years Roadmap of the Sulfur Cathode for Lithium Sulfur Batteries (2009−2020). *Energy Storage Mater.* **2020**, *30*, 346−366.

(8) Shi, L.; Bak, S.; Shadike, Z.; Wang, C. Reaction Heterogeneity in Practical High-Energy Lithium−Sulfur Pouch Cells. *Energy Environ. Sci.* **2020**, *13*, 3620.

(9) Ji, X.; Lee, K. T.; Nazar, L. F. A Highly Ordered Nanostructured Carbon-Sulphur Cathode for Lithium-Sulphur Batteries. *Nat. Mater.* **2009**, *8*, 500−506.

(10) Wang, J.; Yang, J.; Wan, C.; Du, K.; Xie, J.; Xu, N. Sulfur Composite Cathode Materials for Rechargeable Lithium Batteries. *Adv. Funct. Mater.* **2003**, *13*, 487−492.

(11) Tao, X.; Wan, J.; Liu, C.; Wang, H.; Yao, H.; Zheng, G.; Seh, Z. W.; Cai, Q.; Li, W.; Zhou, G.; Zu, C.; Cui, Y. Balancing Surface Adsorption and Diffusion of Lithium-Polysulfides on Nonconductive Oxides for Lithium-Sulfur Battery Design. *Nat. Commun.* **2016**, *7*, 11203.

(12) Mikhaylik, Y. V. Electrolytes for lithium sulfur cells. U.S. Patent 7,352,680 B2, 2008.
(13) Adams, B. D.; Carino, E. V.; Connell, J. G.; Han, K. S.; Cao, R.; Chen, J.; Zheng, J.; Li, Q.; Mueller, K. T.; Henderson, W. A.; Zhang, J.-G. Long Term Stability of Li-S Batteries Using High Concentration Lithium Nitrate Electrolytes. *Nano Energy* **2017**, *40*, 607−617.
(14) Shaibani, M.; Mirshekarloo, M. S.; Singh, R.; Easton, C. D.; Cooray, M. C. D.; Eshraghi, N.; Abendroth, T.; Dörfler, S.; Althues, H.; Kaskel, S.; Hollenkamp, A. F.; Hill, M. R.; Majumder, M. Expansion-Tolerant Architectures for Stable Cycling of Ultrahigh-Loading Sulfur Cathodes in Lithium-Sulfur Batteries. *Sci. Adv.* **2020**, *6*, No. eaay2757.
(15) Liu, H.; Holoubek, J.; Zhou, H.; Chen, A.; Chang, N.; Wu, Z.; Yu, S.; Yan, Q.; Xing, X.; Li, Y.; Pascal, T. A.; Liu, P. Ultrahigh Coulombic Efficiency Electrolyte Enables Li||SPAN Batteries with Superior Cycling Performance. *Mater. Today* **2021**, *42*, 17−28.
(16) Wang, L.; He, X.; Li, J.; Chen, M.; Gao, J.; Jiang, C. Charge/Discharge Characteristics of Sulfurized Polyacrylonitrile Composite with Different Sulfur Content in Carbonate Based Electrolyte for Lithium Batteries. *Electrochim. Acta* **2012**, *72*, 114−119.
(17) Wang, J.; Yang, J.; Xie, J. A Novel Conductive Polymer-Sulfur Composite Material for Rechargeable Lithium Batteries. *Adv. Mater.* **2002**, *14*, 963−965.
(18) Xiang, J.; Guo, Z.; Yi, Z.; Zhang, Y.; Yuan, L.; Cheng, Z.; Shen, Y.; Huang, Y. Facile Synthesis of Sulfurized Polyacrylonitrile Composite as Cathode for High-Rate Lithium-Sulfur Batteries. *J. Energy Chem.* **2020**, *49*, 161−165.
(19) Markevich, E.; Salitra, G.; Chesneau, F.; Schmidt, M.; Aurbach, D. Very Stable Lithium Metal Stripping-Plating at a High Rate and High Areal Capacity in Fluoroethylene Carbonate-Based Organic Electrolyte Solution. *ACS Energy Lett.* **2017**, *2*, 1321−1326.
(20) Zhang, Y.; Zhong, Y.; Shi, Q.; Liang, S.; Wang, H. Cycling and Failing of Lithium Metal Anodes in Carbonate Electrolyte. *J. Phys. Chem. C* **2018**, *122*, 21462−21467.
(21) Lv, D.; Zheng, J.; Li, Q.; Xie, X.; Ferrara, S.; Nie, Z.; Mehdi, L. B.; Browning, N. D.; Zhang, J. G.; Graff, G. L.; Liu, J.; Xiao, J. High Energy Density Lithium-Sulfur Batteries: Challenges of Thick Sulfur Cathodes. *Adv. Energy Mater.* **2015**, *5*, 1402290.
(22) Zhang, Y. Z.; Liu, S.; Li, G. C.; Li, G. R.; Gao, X. P. Sulfur/Polyacrylonitrile/Carbon Multi-Composites as Cathode Materials for Lithium/Sulfur Battery in the Concentrated Electrolyte. *J. Mater. Chem. A* **2014**, *2*, 4652−4659.
(23) Zhang, S. Understanding of Sulfurized Polyacrylonitrile for Superior Performance Lithium/Sulfur Battery. *Energies* **2014**, *7*, 4588−4600.
(24) Xing, X.; Li, Y.; Wang, X.; Petrova, V.; Liu, H.; Liu, P. Cathode Electrolyte Interface Enabling Stable Li−S Batteries. *Energy Storage Mater.* **2019**, *21*, 474−480.
(25) Yang, H.; Guo, C.; Chen, J.; Naveed, A.; Yang, J.; Nuli, Y.; Wang, J. An Intrinsic Flame-Retardant Organic Electrolyte for Safe Lithium-Sulfur Batteries. *Angew. Chem. Int. Ed.* **2019**, *58*, 791−795.
(26) Yin, L.; Wang, J.; Yu, X.; Monroe, C. W.; NuLi, Y.; Yang, J. Dual-Mode Sulfur-Based Cathode Materials for Rechargeable Li-S Batteries. *Chem. Commun.* **2012**, *48*, 7868−7870.
(27) Zhao, C.-X.; Chen, W.; Zhao, M.; Song, Y.; Liu, J.; Li, B.; Yuan, T.; Chen, C.; Zhang, Q.; Huang, J. Redox Mediator Assists Electron Transfer in Lithium−Sulfur Batteries with Sulfurized Polyacrylonitrile Cathodes. *EcoMat* **2021**, *3*, No. e12066.
(28) Holoubek, J.; Yu, M.; Yu, S.; Li, M.; Wu, Z.; Xia, D.; Bhaladhare, P.; Gonzalez, M. S.; Pascal, T. A.; Liu, P.; Chen, Z. An All-Fluorinated Ester Electrolyte for Stable High-Voltage Li Metal Batteries Capable of Ultra-Low-Temperature Operation. *ACS Energy Lett.* **2020**, *5*, 1438−1447.
(29) Philippe, B.; Hahlin, M.; Edström, K.; Gustafsson, T.; Siegbahn, H.; Rensmo, H. Photoelectron Spectroscopy for Lithium Battery Interface Studies. *J. Electrochem. Soc.* **2016**, *163*, A178−A191.
(30) Frey, M.; Zenn, R. K.; Warneke, S.; Müller, K.; Hintennach, A.; Dinnebier, R. E.; Buchmeiser, M. R. Easily Accessible, Textile Fiber-Based Sulfurized Poly(Acrylonitrile) as Li/S Cathode Material: Correlating Electrochemical Performance with Morphology and Structure. *ACS Energy Lett.* **2017**, *2*, 595−604.
(31) Hu, Y.; Li, B.; Jiao, X.; Zhang, C.; Dai, X.; Song, J. Stable Cycling of Phosphorus Anode for Sodium-Ion Batteries through Chemical Bonding with Sulfurized Polyacrylonitrile. *Adv. Funct. Mater.* **2018**, *28*, 1801010.
(32) Feng, X.; Song, M.-K.; Stolte, W. C.; Gardenghi, D.; Zhang, D.; Sun, X.; Zhu, J.; Cairns, E. J.; Guo, J. Understanding the Degradation Mechanism of Rechargeable Lithium/Sulfur Cells: A Comprehensive Study of the Sulfur-Graphene Oxide Cathode after Discharge-Charge Cycling. *Phys. Chem. Chem. Phys.* **2014**, *16*, 16931−16940.
(33) Li, X.; Banis, M.; Lushington, A.; Yang, X.; Sun, Q.; Zhao, Y.; Liu, C.; Li, Q.; Wang, B.; Xiao, W.; Wang, C.; Li, M.; Liang, J.; Li, R.; Hu, Y.; Goncharova, L.; Zhang, H.; Sham, T. K.; Sun, X. A High-Energy Sulfur Cathode in Carbonate Electrolyte by Eliminating Polysulfides via Solid-Phase Lithium-Sulfur Transformation. *Nat. Commun.* **2018**, *9*, 4509.
(34) Fanous, J.; Wegner, M.; Grimminger, J.; Andresen, Ä.; Buchmeiser, M. R. Structure-Related Electrochemistry of Sulfur-Poly(Acrylonitrile) Composite Cathode Materials for Rechargeable Lithium Batteries. *Chem. Mater.* **2011**, *23*, 5024−5028.
(35) Wang, X.; Qian, Y.; Wang, L.; Yang, H.; Li, H.; Zhao, Y.; Liu, T. Sulfurized Polyacrylonitrile Cathodes with High Compatibility in Both Ether and Carbonate Electrolytes for Ultrastable Lithium−Sulfur Batteries. *Adv. Funct. Mater.* **2019**, *29*, 1902929.
(36) Wang, W.; Cao, Z.; Elia, G. A.; Wu, Y.; Wahyudi, W.; Abou-Hamad, E.; Emwas, A.-H.; Cavallo, L.; Li, L.-J.; Ming, J. Recognizing the Mechanism of Sulfurized Polyacrylonitrile Cathode Materials for Li-S Batteries and beyond in Al-S Batteries. *ACS Energy Lett.* **2018**, *3*, 2899−2907.
(37) Wei, S.; Ma, L.; Hendrickson, K. E.; Tu, Z.; Archer, L. A. Metal-Sulfur Battery Cathodes Based on PAN-Sulfur Composites. *J. Am. Chem. Soc.* **2015**, *137*, 12143−12152.
(38) Li, W.; Yao, H.; Yan, K.; Zheng, G.; Liang, Z.; Chiang, Y. M.; Cui, Y. The Synergetic Effect of Lithium Polysulfide and Lithium Nitrate to Prevent Lithium Dendrite Growth. *Nat. Commun.* **2015**, *6*, 7436.
(39) Farges, F.; Keppler, H.; Flank, A.-M.; Lagarde, P. Sulfur K-Edge XANES Study of S Sorbed onto Volcanic Ashes. *J. Phys. Conf.* **2009**, *190*, 012177.
(40) Ye, Y.; Kawase, A.; Song, M. K.; Feng, B.; Liu, Y. S.; Marcus, M. A.; Feng, J.; Cairns, E. J.; Guo, J.; Zhu, H. J. X-Ray Absorption Spectroscopy Characterization of a Li/S Cell. *Nanomaterials* **2016**, *6*, 14.
(41) Gorlin, Y.; Siebel, A.; Piana, M.; Huthwelker, T.; Jha, H.; Monsch, G.; Kraus, F.; Gasteiger, H. A.; Tromp, M. Operando Characterization of Intermediates Produced in a Lithium-Sulfur Battery. *J. Electrochem. Soc.* **2015**, *162*, A1146−A1155.
(42) Dominko, R.; Patel, M. U. M.; Lapornik, V.; Vizintin, A.; Koželj, M.; Stievano, L.; Aquilanti, G.; Aquilanti, G. Analytical Detection of Polysulfides in the Presence of Adsorption Additives by Operando X-Ray Absorption Spectroscopy. *J. Phys. Chem. C* **2015**, *119*, 19001−19010.
(43) Gao, Y.; Yan, Z.; Gray, J. L.; He, X.; Wang, D.; Chen, T.; Huang, Q.; Li, Y. C.; Wang, H.; Kim, S. H.; Mallouk, T. E.; Wang, D. Polymer−Inorganic Solid−Electrolyte Interphase for Stable Lithium Metal Batteries under Lean Electrolyte Conditions. *Nat. Mater.* **2019**, *18*, 384−389.
(44) Niu, C.; Pan, H.; Xu, W.; Xiao, J.; Zhang, J.-G.; Luo, L.; Wang, C.; Mei, D.; Meng, J.; Wang, X.; Liu, Z.; Mai, L.; Liu, J. Self-Smoothing Anode for Achieving High-Energy Lithium Metal Batteries under Realistic Conditions. *Nat. Nanotechnol.* **2019**, *14*, 594−601.
(45) Liu, H.; Wang, X.; Zhou, H.; Lim, H.-D.; Xing, X.; Yan, Q.; Meng, Y. S.; Liu, P. Structure and Solution Dynamics of Lithium Methyl Carbonate as a Protective Layer for Lithium Metal. *ACS Appl. Energy Mater.* **2018**, *1*, 1864−1869.
(46) Liu, H.; Yue, X.; Xing, X.; Yan, Q.; Huang, J.; Petrova, V. A Scalable 3D Lithium Metal Anode. *Energy Storage Mater.* **2019**, *16*, 505−511.

https://doi.org/10.1021/acsami.1c07903
ACS Appl. Mater. Interfaces 2021, 13, 31733−31740